6-2023

On the Measurement of Nakazima Testing Based Out-of-Plane Forming Limit Curves using 2D Digital Image Correlation

Akshat Agha

Fadi Abu-Farha

International Journal of Pioneering Technology and Engineering

Research Article

On the Measurement of Nakazima Testing Based Out-of-Plane Forming Limit Curves using 2D Digital Image Correlation

Akshat Agha[a]* **Fadi Abu-Farha**[a]

[a] FADI-AMT LLC, Greenville, SC 29607, USA

Article Info

Article history
Received: 18/04/2023
Revised: 14/05/2022
Accepted: 26/05/2023

Keywords:
Sheet Metal Forming,
Nakazima Testing,
Forming Limit Curve,
Stamping,
Full-field Strain.

ABSTRACT

The strain compensation method for measuring in-plane forming limit curves (FLCs) using 2D digital image correlation developed previously [A method of measuring in-plane forming limit curves using 2D Digital Image Correlation, SAE Int. J. Mater. Manf., 2023] was modified and extended to more versatile and popular out-of-plane FLCs. The current study introduces a straightforward strain compensation technique for measuring Nakazima testing based out-of-plane FLCs utilizing an affordable single-camera (2D) DIC system. In this study, forming tests are performed on two automotive-grade sheet metal alloys: DP980 steel and a 6xxx series aluminum alloy using the Nakazima test method. The experiments are conducted on a customized setup that allows for simultaneous optical strain measurements using both a stereo DIC and a 2D DIC system. The FLCs are obtained by applying a temporal FLC computation approach to the two measurement sets. The results show that 2D DIC FLC points match those obtained by stereo DIC for both the materials after applying the proposed strain correction method.

1. Introduction

The sheet metal forming industry heavily relies on Forming Limit Curves (FLCs) and Forming Limit Diagrams (FLDs) of sheet metal alloys, which determine the maximum amount of stretching a sheet metal can withstand during the stamping process. An FLD consists of strain pair clouds (major strain $\epsilon 1$, minor strain $\epsilon 2$) categorized into safe, marginal, and failure regions. The crucial element of an FLD is the forming limit curve or FLC, which identifies the limit of unstable necking, represented by the red line on the plot. FLCs can be obtained through theoretical or experimental methods. However, predicting FLCs through theory has become increasingly challenging due to the complex microstructures of advanced materials.

Experimental FLCs are generated by mechanical stretching tests, with the most widely used tests being the Marciniak in-plane stretching tests [1] and Nakazima ball punch stretching tests [2]. The current state of the art involves integrating a stereo Digital Image Correlation (DIC) system with formability tests. The usage of DIC in formability testing provides the strain history on the surface of the test sample deformation until rupture, which can be post-processed using mathematical computations to determine the necking limits.

Both Marciniak and Nakazima tests require out-of-plane translation of the test sample, which is why stereo DIC has always been the preferred choice for conducting such tests. However, 2D DIC was never deemed suitable for formability testing due to the potential errors associated with out-of-plane translation of the test sample or camera. While the use of stereo DIC for formability testing offers many advantages, the high cost of commercial stereo DIC systems remains a significant obstacle to their widespread use, particularly in academic institutions where it represents a substantial investment. In this aspect, if there is a way to overcome the errors associated with out-of-plane translation in a 2D DIC measurement, it will clear the path forward for the mass adoption of DIC for formability testing. In a previous publication [3], the authors showed that, if performed correctly, 2D DIC measurements can match the stereo DIC measurements even for large local strains (fracture strains). In addition to that, the authors have previously presented a simple compensation method for obtaining accurate and reliable in-plane FLCs from Marciniak tests using a single-camera DIC system [4]. Their method could not work on out-of-plane Nakazima tests, which are highly adopted and more popular in the sheet metal forming industry. This work addresses that gap and proposes a material-independent, simple, and easy-to-implement 2D DIC strain compensation method for the determination of FLCs from out-of-plane Nakazima ball punch tests.

In this work, formability tests using the Nakazima method are performed on two popular automotive-grade sheet metal alloys using a custom test setup that enables simultaneous optical measurements using a stereo DIC and a 2D DIC system. The FLCs are generated using the time-dependent Linear Best Fit (LBF) method. Finally, the FLCs obtained through the strain compensation method on 2D DIC measurements are validated against the benchmark FLCs produced by the stereo DIC measurements.

***Corresponding author:** Akshat Agha
*E-mail address: akshat@fadi-amt.com
https://doi.org/10.56158/jpte.2023.42.2.01

2. Material and Method

2.1. Material

The study was performed on two materials relevant to the automotive industry. The first material is a 1.6 mm thick Dual-phase 980 MPa (DP980) steel that is used for structural applications, and the second material is a 1.0 mm thick AA6xxx series aluminum alloy (AL6) that is used for vehicle enclosures. The mechanical properties of the two materials were obtained through uniaxial tension tests performed using ISO 6892-Method B standard (plotted in Figure 1).

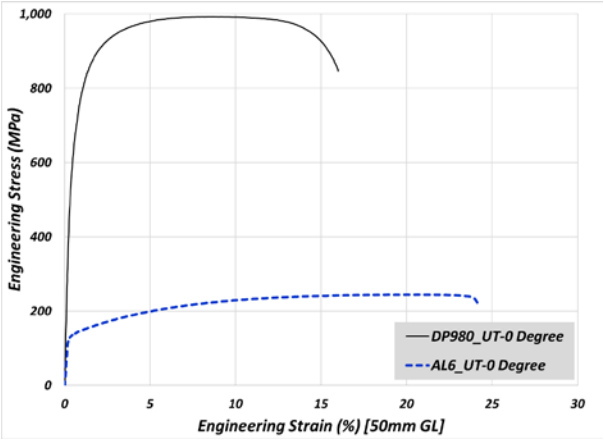

Fig. 1. Uniaxial Tension Stress-Strain curves of DP980 (1.6 mm thick) and AL6 (1.0 mm thick)

2.2. Experimental Setup

The experimental test configuration comprises a custom-built servo-hydraulic press capable of clamping (binder) up to 1800 kN and punch capacity up to 1000 kN. To allow for the DIC cameras to view the test sample during testing, the top plate of the press features a circular cut-out. As illustrated in Figure 2, the 2D DIC and stereo DIC cameras are positioned on top of the press. The 2D DIC utilizes custom-built hardware (employing an 8MP CMOS camera with appropriate optics) to observe the test sample in normal orientation, while the stereo DIC employs a commercial 6MP system.

The FLCs were determined using Nakazima ball punch tests following the ISO 12004-2:2021 standard. The Nakazima method is an out-of-plane test where the test sample is deformed in the shape of a dome until it fails. The test samples were clamped using 1200 kN for DP980, and 800 kN binder force for AL6 before being deformed with a circular ball punch (4" diameter) moving at a constant punch velocity of 1.0 mm/s.

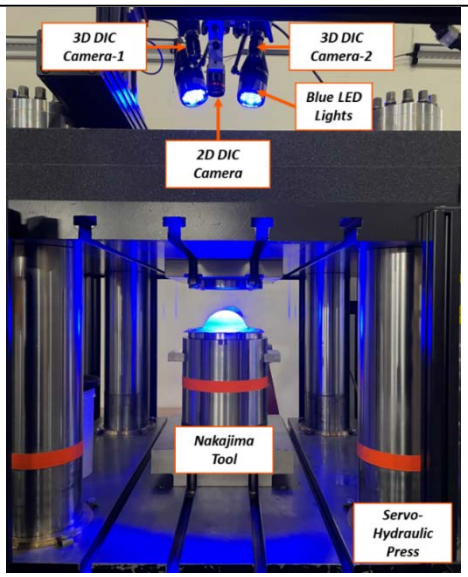

Fig. 2. Nakazima test setup showing a servo-hydraulic press equipped with a top-mounted 2D and stereo DIC system

2.3. Test Samples Geometries

The sample geometries used for Nakazima tests were prepared per the ISO12004 standard. At least 7 different geometries were tested for each material, and at least three repeats were tested per geometry (Figure 3) to ensure the repeatability of the results. The samples were waterjet cut and it was ensured that the gage region was aligned with the rolling direction of the sheet material in the case of AL6 and perpendicular to the rolling direction for the DP980 steel (as per the recommendation for the specified in the ISO standard, RD is the conservative direction for aluminum alloys, and TD is the conservative direction for steels). A layer of PTFE foil and grease was applied between the test sample and the ball punch to minimize the effect of friction and enable uniform stretching in the center of the test sample. To facilitate DIC tracking, black-and-white speckle patterns were generated on the surface of the test samples using regular matte paints.

2.4. DIC Setup

The stereo DIC system was calibrated as per the manufacturer's standard procedure. On the other hand, the bespoke 2D DIC system was calibrated using an image of a scale bar placed at the plane of the undeformed sample. Table 1 lists the key parameters that affect DIC measurements, and their meanings are described in the subsequent sections.

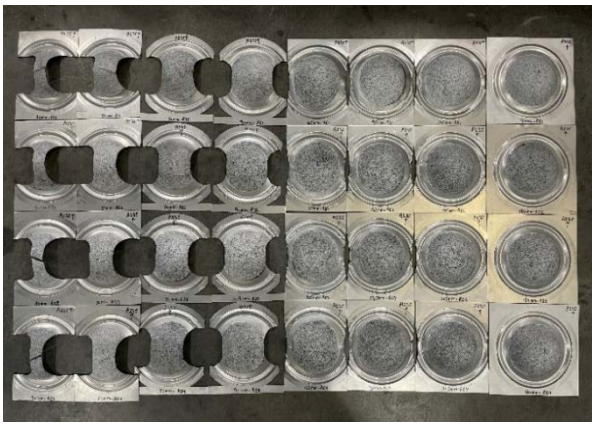

Fig. 3. Full set of Nakazima test samples

2.4.1. Pixel Resolution

The resolution of the DIC measurements, which indicates the relationship between the physical length in the field of view and the number of pixels, is known as the spatial resolution and is

expressed in microns per pixel. To ensure that the two systems used in this study had similar spatial resolutions, the camera optics for each system were selected with care. The spatial resolutions of the 2D DIC and stereo DIC setups were 49 and 45 microns/pixel, respectively, and these values were deemed comparable enough to compare the strain results obtained from the two systems.

2.4.2. Acquisition Frame Rate

As per ISO 12004-2 standard, a minimum image acquisition rate of 10 frames per mm of punch displacement is necessary, which corresponds to at least 10 Hz for a test speed of 1.0 mm/s. For this study, a frame rate of 20 Hz was selected for both the DIC systems. The two camera systems were configured to accept a digital signal, allowing for automatic triggering at the beginning of the test. By synchronizing the auto-trigger and the camera frame rate settings, it was possible to capture images with identical timestamps, facilitating a direct comparison of the test results.

2.4.3. Virtual Strain Gauge Length (VSGL)

The VSGL is the length over which the DIC software calculates the displacement and strain fields. A smaller VSGL picks up higher local strains which can show as noise or hotspots in the measurements, while larger VSGL results in higher averaging and smoothened strain results. In this study, the DIC algorithm was run for a VSGL of 1 mm, and the subset size and spacing were adjusted accordingly. This ensured that the strain calculations were consistent between the 2D and stereo DIC systems. The strain interpolation and neighborhood averaging were also matched to ensure consistency between the two systems.

Table 1. Optical System Details and DIC Processing Parameters

	Stereo DIC	***2D DIC***
System Type	Commercial	Custom-Built
Cameras	2 x 6 MP	1 x 8 MP
Frame Rate (Hz)	20	20
Resolution (pixels x pixels)	2752x2200	2840x2840
Measuring Distance Z (mm)	~550	~480
Pixel Resolution (microns/pixel)	~39	~41
Subset Size (pixels)	35x35	35x35
Subset Spacing (pixels)	13	13
Virtual Strain Gauge Length (mm)	~1	~1
Interpolation	Bicubic	Bicubic
Facet Matching	Against Ref. Frame	Against Ref. Frame

3. Investigations on DIC Generated Experimental Results

After the DIC processing, full-field surface contour maps were exported for each frame. A sample Z-displacement contour map (from stereo DIC) for a DP980 test sample, representing the balanced biaxial stretching, is shown in Figure 4(a). This map was taken for the last frame before rupture, and it shows that the test sample deforms in an out-of-plane condition. The Z-displacement distribution along a vertical section drawn on the DIC correlated area (Figure 4(b)) shows that the Nakazima test sample deformed out-of-plane and the apex of the dome reached a height of ~29 mm. The entire deformation zone of the Nakazima test sample stretched to different heights (unlike Marciniak tests, where the entire deformation zone stays in-plane), which makes it difficult to estimate the Z-displacement on the different locations on the gauge area of the sample. For the method proposed later, it is important to estimate the Z-displacement at the rupture area.

For the evaluation of the strain profile on the Nakazima test sample, the major strain contour map (from stereo DIC) for a DP980 test sample, representing the balanced biaxial stretching, is shown in Figure 5(a). This contour plot captured at the last frame before rupture exhibits the strain concentration and thinning in the center of the sample (as desired for FLC points extraction). A vertical cross-section was drawn on the major strain contour, and the major strain distribution on the cross-section was compared for the two DIC systems. The strain distributions from the two DIC systems along the vertical section shown in Figure 5(b) are widely different.

Figure 6 shows an example of major strain contour maps obtained from the two DIC systems for a balanced biaxial tension test sample of DP980 Steel at the same timestamp, right before rupture. As observed, the strain distribution at the apex of the specimen appears comparable between the two DIC systems, provided that the legends of the two plots are suitably adjusted. Based on the results of Figure 5 b) and Figure 6, The strains recorded by the 2D DIC in the region close to the apex of the dome are higher than the stereo DIC results, however, they tend to go lower in the periphery of the selected circular region, away from the dome apex.

The above-mentioned phenomenon is a combined effect of three complex behaviors:

(i) Positive strain due to out-of-plane translation: There is an artificial positive strain added to the measurements due to the out-of-plane translation of the entire sample towards the camera, but unlike the Marciniak tests, these artificial strain values are not the same for the entire deformation zone. The apex region of the dome being closest to the camera accumulates higher artificial strain and the artificial strain values decrease with the distance from the apex region.

(ii) Negative strain due to out-of-plane rotation: As the test sample deforms, the subsets in the apex region experience stretching with minimal out-of-plane rotation, while the subsets away from the apex region lying in the periphery of the selected circular region experience rotation with respect to the camera plane. Due to the inability of the 2D DIC to capture out-of-plane rotation, this rotation in the subsets is perceived as compression. This adds artificial negative strain to the areas away from the dome apex.

(iii) Change in section length: The length of the vertical section drawn on the sample increases with the deformation. In the case of stereo DIC results, the increased section length is perceived as the circumference of the dome. However, for 2D DIC, the section length stays the same, which affects the shape of the parabolic true strain vs. section length plot as shown in Figure 5 b).

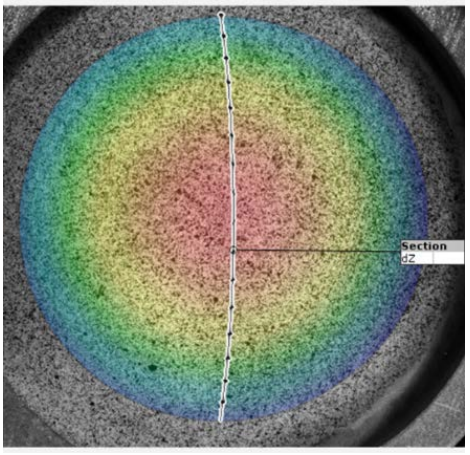

a)

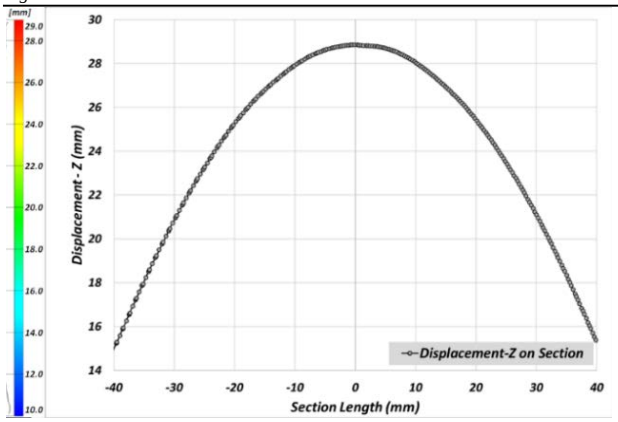

b)

Fig. 4. a) Z-Displacement (mm) contour map and a vertical section at the last frame before rupture on a DP980 steel balanced biaxial tension test sample; b) Z-Displacement (mm) along the vertical section drawn on the test sample

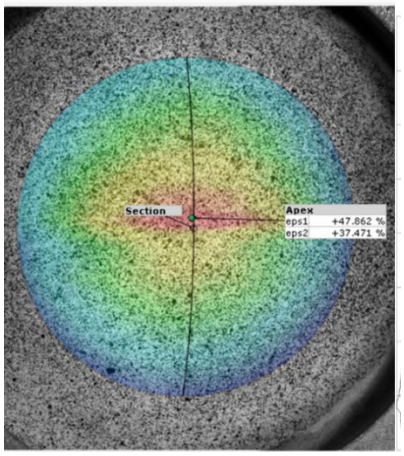

a)

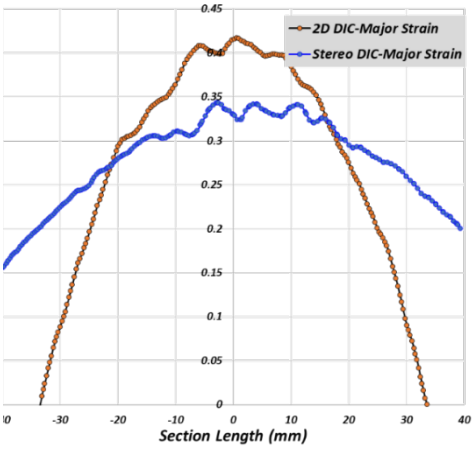

b)

Fig. 5. a) Major strain contour map and a vertical section at the last frame before rupture on a DP980 steel balanced biaxial tension test sample; b) Major strain distribution along the vertical section obtained from the 2D DIC and stereo DIC

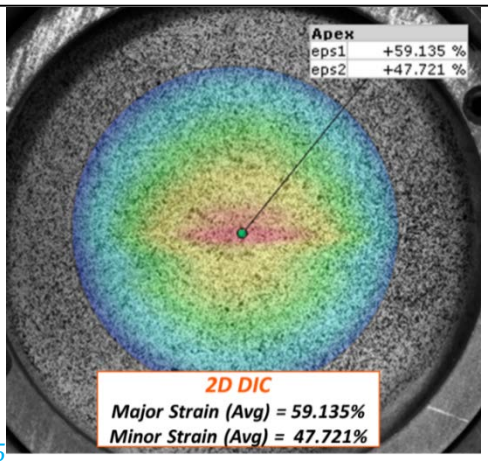

a)

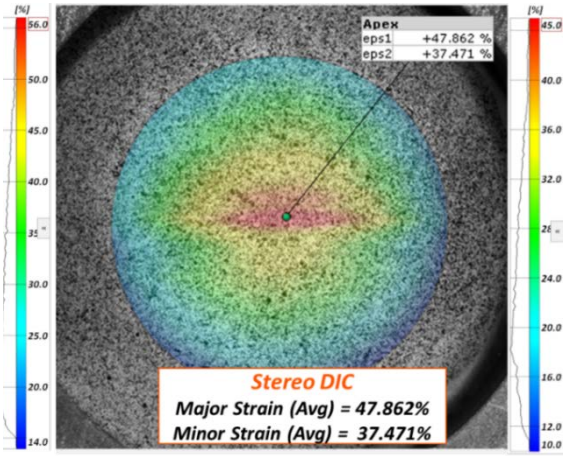

b)

Fig. 6. Major strain contour maps for a balanced biaxial tension test sample of DP980 steel at the same timestamp obtained using 2D DIC and stereo DIC

The ISO 12004-2 standard states that, “For the test to be valid, the fracture shall occur within a distance less than 15 % of the punch diameter away from the apex of the dome. Specimen not meeting this requirement shall be rejected”. In our case, the test sample must fail within 15 mm of the apex of the dome. On investigating the z-displacement contour map of the DP980 test sample, it is seen that all the points within a 15 mm radius of the apex lie within 2 mm of Z-displacement, as shown in Figure 7. It can be mathematically calculated that even for materials with very high stretchability, the maximum variation of Z-displacement in the 15 mm sphere cannot exceed 2.3 mm. Therefore, for a good test sample, the Z-displacement of the rupture area can be assumed to be the same as the Z-displacement of the dome apex i.e., punch displacement. The aforementioned observation plays a crucial role in the 2D DIC error compensation technique put forth in this study.

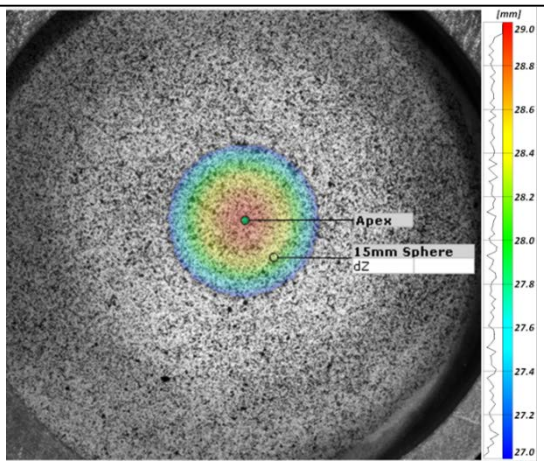

Fig. 7. Z-Displacement (mm) contour map in a 15 mm sphere around the apex of the dome of the DP980 steel balanced biaxial tension test sample

4. FLC Computation Approach

There are several FLC evaluation approaches to convert the major-minor strain pairs into critical FLC points. These mathematical approaches can be broadly divided into three categories – spatial methods (like ISO 12004-2:2021 section-based method [5]), temporal or time-dependent methods ([6]–[9]), and spatio-temporal hybrid methods ([10]–[12]). Hotz et al. [8], Min et al.[13] and Huang et al.[14] can be referred to for a detailed comparison of the different FLC computation approaches.

The strain compensation method proposed in the next section can reliably correct the strain error induced due to the out-of-plane translation but cannot fix the errors induced due to the rotation or section length. Therefore, in this work, we focus on the popular time-dependent Linear Best Fit method because it depends solely on the strain history in the rupture zone that lies on the dome apex or at least within 15 mm of the dome apex.

4.1. Linear Best Fit (LBF) Method

In 2011, Volk and Hora [15] introduced the LBF technique to detect instability, which relies on a time-dependent approach. According to their method, the onset of instability is indicated by a significant increase in thinning strains in a defined necking region.

For this investigation, the necking area is defined as the set of all subsets that exhibit an effective strain value greater than 90% of the maximum effective strain observed on the specimen in the final frame before failure., as shown in Figure 8. The major (ε_1) and minor (ε_2) strain values are obtained by averaging over the necking region for each frame for the entire deformation history, while thickness strain (ε_3) is determined using the volume constancy law.

The thickness strain is differentiated with respect to displacement to obtain the thinning rate which is then averaged over a moving window of 7 points to reduce the effect of noise. The computation is carried out on the frames corresponding to the final 4 mm of punch displacement leading up to the point of rupture. Given the 20 Hz camera acquisition rate adopted in this investigation, a total of 80 images are utilized in the LBF calculation. Figure 9 depicts major, minor, and thinning strains, as well as thinning rate, in relation to punch displacement within the final 4 mm. The technique incorporates a stable line fit, which is a linear fit between punch displacement of -4 mm and -2 mm, and an unstable line fit, which is a linear fit for the last 7 points before rupture. The intersection of these two lines is considered the critical point in time when unstable necking is presumed to have started, thus the major/minor strain values at this point are recognized as an FLC point.

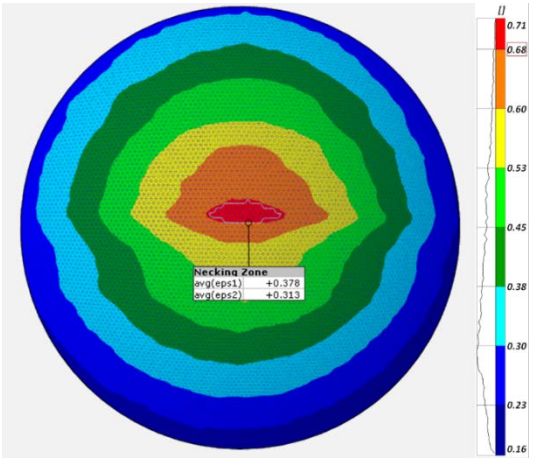

Fig. 8. Effective strain contour map and necking zone selection on a balanced biaxial test sample

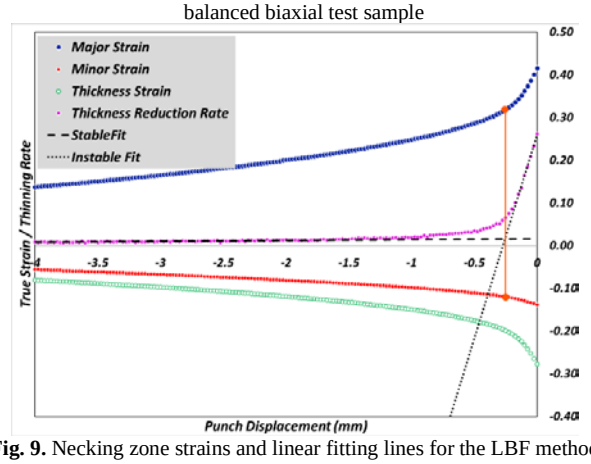

Fig. 9. Necking zone strains and linear fitting lines for the LBF method plotted for the last 4 mm of punch travel

5. Out-Of-Plane Error Compensation in 2D DIC

The underlying principle of a pinhole camera states that an object appears larger when it is nearer to the camera, and smaller when it is farther away. This means that measurements taken using a 2D DIC technique are susceptible to inaccuracies if the distance between the camera and the test sample changes. Specifically, a drop in the measuring distance results in artificial positive strains, and a drop in the measuring distance results in negative artificial strains. Fortunately, the error in the measurement due to the artificial strains is systematic, quantifiable, and removable.

It is mathematically derived that the artificial strain introduced into the measurements by the sample's out-of-plane displacement is proportional to the ratio of the change in measuring distance (Δz) and the initial measuring distance (z) [16].

As per the observation made in section 3, the failure area in a Nakazima test sample is within 2 mm of Z-displacement, i.e., the failure region of a 15 mm radius around the apex can be assumed to be in the same plane. The effects of this simplification will be evaluated in the discussion section. This means that if the Z-displacement of the apex (or dome height) is known, the error in the 2D DIC measurements for Nakazima tests can be calculated and removed for all the points within the failure zone.

Figure 10 shows a schematic of the Nakazima FLC test setup with 2D DIC. The change in measuring distance is equal to the dome height (Δz), which in this case, is a function of the punch speed and test time recorded by the DIC system, as given in eq. (1). The corrected strain can be calculated by removing the artificial strain from the 2D DIC measured strains using eq. (2).

$$\Delta z = Punch\ Speed\ x\ Test\ Time \quad (1)$$

$$\in (\%)_{corrected} = \in (\%)_{measured} - \frac{\Delta z}{z}(\%) \quad (2)$$

In the current investigation, the punch velocity was 1.0 mm/s, and this value was multiplied by the duration of the test (per frame) to calculate the dome height (Δz) for that frame. The initial measuring distance (z) between the lens of the 2D DIC system and the test sample plane is 480 mm (as shown in Table 1). By employing these two formulas, the artificial strain was estimated for each frame and subsequently eliminated from the measurements.

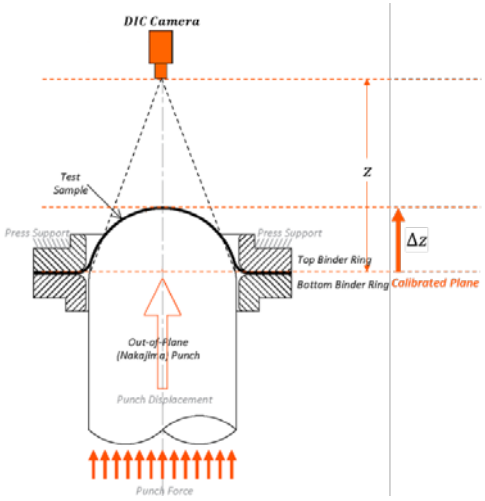

Fig. 10. Schematic of the Nakazima FLC test setup with 2D DIC showing a deforming sample translating closer to the camera and away from the 2D DIC calibrated plane

6. FLC Results

It is essential to highlight that in this study, the stereo DIC-generated FLC is used as a benchmark, and the 2D DIC outcomes are evaluated against it.

6.1. FLC by the LBF Method

The LBF method involves fitting a non-linear quantity (thinning rate), therefore, the correction outlined in the previous section was first applied to the major-minor strain pairs for each frame before applying the LBF FLC computation method described in section 4. The LBF fitting was handled by a custom-written Python script. The FLCs generated by the 2D DIC system using the LBF method, before and after correction, are plotted against those obtained by the stereo DIC system, shown in Figure 11-12 for DP980 steel, and Figure 13-14 for AL6 aluminum alloy. The FLC points obtained from 2D DIC after correction show excellent agreement with the stereo DIC points for both materials.

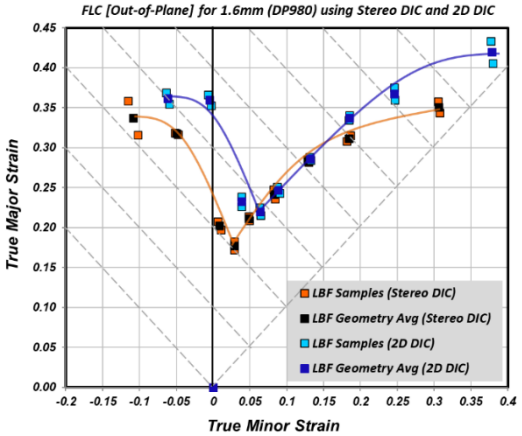

Fig. 11. Out-of-Plane FLCs for DP980 steel using 2D DIC (before correction) and stereo DIC

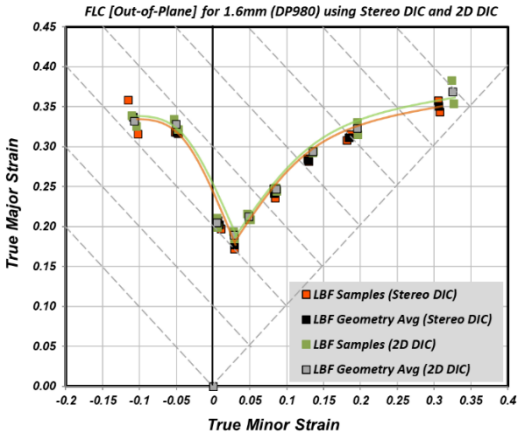

Fig. 12. Out-of-Plane FLCs for DP980 steel using 2D DIC (after correction) and stereo DIC

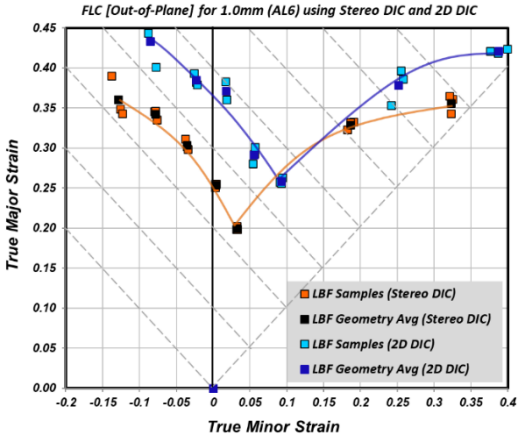

Fig. 13. Out-of-Plane FLCs for AL6 using 2D DIC (before correction) and stereo DIC

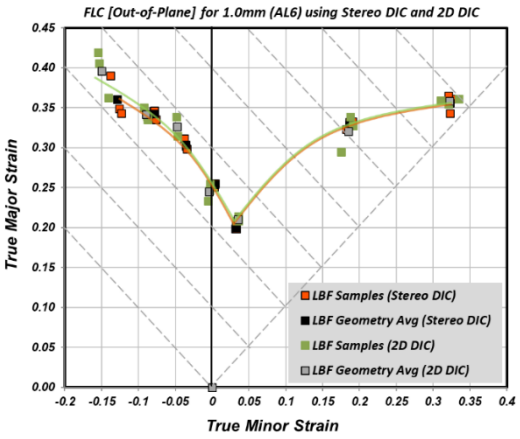

Fig. 14. Out-of-Plane FLCs for AL6 using 2D DIC (after correction) and stereo DIC

7. Discussion

In the proposed method, it is assumed that there is a negligible difference in the Z-displacement of all the points within the 15 mm distance of the dome apex, and it is considered equal to the dome height. The effect of this assumption is negligible, and it is clear from the results presented in the above plots. It can be explained mathematically that the effect of this local height variation is insignificant - the initial measuring distance in our case study is 480 mm, for a balanced biaxial tension test sample with a dome height of 29 mm, the artificially added strain due to the out-of-plane translation is 0.059 (true strain) in the major strain as well as minor strain. Let's assume that the failure in the test specimen happens off-center at the farther acceptable distance of 15 mm from the dome apex and

the actual Z-displacement at the failure location was 27 mm. It means that the actual error in the test sample was 0.055 (true strain). In this case, the proposed algorithm, over-compensates the strains by 0.004 strains, which is negligible on the scale of the FLC plot. Therefore, the errors in the out-of-plane FLC results are not noticeable.

The proposed method is shown to work with two varying classes of materials – DP980 steel and AL6 aluminum alloy. In addition to that, the algorithm presented in this work is material-independent and works with any material that can be reliably tested using the Nakazima ball punch method.

It has been demonstrated that the proposed method is effective for the time-dependent LBF approach, and it can be extended to other time-dependent techniques. However, due to the inability of the 2D DIC to perceive any out-of-plane rotation or changes in the section length, the proposed method doesn't work on spatial methods of FLC computation. Also, this study does not challenge or recommend any specific FLC computation method, and the main intent here is to prove that the same FLC can be obtained from a 2D DIC.

8. Conclusions

This paper presents a method for enabling experimental determination of Nakazima testing based on out-of-plane Forming Limit Curve (FLC) for sheet metal alloys using a low-cost 2D Digital Image Correlation (DIC) system. The method was tested on tests performed on a 1.6 mm thick DP980 steel and a 1.0 mm thick AL6 aluminum alloy using a custom-built test configuration that enabled simultaneous strain measurements using stereo DIC and 2D DIC systems. The FLC points were determined using a popular and well-accepted time-dependent method – LBF. After implementing the proposed correction to 2D DIC strains, the resulting FLCs exhibited satisfactory consistency with the FLCs derived from a stereo DIC system.

The findings provide evidence that a single-camera DIC system can precisely ascertain an out-of-plane FLC for a sheet metal alloy. It should be noted that this work does not advocate for replacing stereo DIC systems with 2D DIC systems. Instead, the aim is to facilitate the widespread adoption of DIC in budget-limited environments, thus leveraging the benefits of optical metrology over traditional FLC determination methods without the need for substantial investments in stereo DIC systems.

The proposed method of strain correction is intended for Nakazima ball punch tests processed using time-dependent methods. The correction method would need further investigations for other FLC computation approaches, and that is a topic for future study.

8.1. Appendix: FLC Data Points for DP980 and AL6

Tables 2 and 3 below show the FLC points for 1.6 mm thick DP980 steel and 1.0 mm AL6 aluminum alloy obtained from the stereo DIC and 2D DIC (before and after correction).

Table 2. LBF method based FLC Points (geometry averages) for 1.6 mm thick DP980 steel

FLC Points for DP980						
#	*Stereo DIC*		*2D DIC*		*2D DIC (corrected)*	
	ε1 mean (log.)	*ε2 mean (log.)*	*ε1 mean (log.)*	*ε2 mean (log.)*	*ε1 mean (log.)*	*ε2 mean (log.)*
1	0.337	-0.109	0.362	-0.062	0.332	-0.107
2	0.318	-0.050	0.360	-0.005	0.328	-0.050
3	0.202	0.009	0.233	0.039	0.205	0.005
4	0.177	0.029	0.220	0.064	0.190	0.028
5	0.211	0.049	0.247	0.089	0.213	0.048
6	0.242	0.083	0.286	0.132	0.247	0.086
7	0.283	0.129	0.337	0.185	0.294	0.136
8	0.312	0.184	0.367	0.246	0.323	0.196
9	0.351	0.306	0.420	0.378	0.369	0.325

Table 3. LBF method based FLC Points (geometry averages) for 1.0 mm thick AL6 aluminum alloy

FLC Points for AL6						
#	*Stereo DIC*		*2D DIC*		*2D DIC (corrected)*	
	ε1 mean (log.)	*ε2 mean (log.)*	*ε1 mean (log.)*	*ε2 mean (log.)*	*ε1 mean (log.)*	*ε2 mean (log.)*
1	0.361	-0.129	0.433	-0.086	0.396	-0.150
2	0.342	-0.078	0.385	-0.023	0.341	-0.089
3	0.304	-0.036	0.372	0.017	0.326	-0.048
4	0.254	0.003	0.292	0.056	0.245	-0.004
5	0.200	0.032	0.259	0.092	0.210	0.035
6	0.329	0.186	0.379	0.251	0.320	0.185
7	0.356	0.323	0.421	0.387	0.358	0.322

Declaration of conflicting interests

The authors declare no competing interests.

Funding

The author received no financial support for the research and/or authorship of this article.

References

[1] Marciniak Z. and Kuczyński K., 1967, *Limit strains in the processes of stretch-forming sheet metal*, Int J Mech Sci, vol. 9, no. 9, pp. 609–620, Sep., doi: 10.1016/0020-7403(67)90066-5.

[2] Nakazima, K., Toshio Kikuma, and Kaname Hasuka, 1968, *Study on the formability of steel sheets*, Yawata Tech Rep, Sept, vol. 264, pp. 8517–8530, 1968.

[3] Agha A., 2022, *Effectiveness of 2D Digital Image Correlation in Capturing the Fracture Behavior of Sheet Metal Alloys*, SAE International Journal of Materials and Manufacturing, vol. 16, no. 2, doi: 10.4271/05-16-02-0009.

[4] A. Agha and F. Abu-Farha, 2023, *A Method for Measuring In-Plane Forming Limit Curves Using 2D Digital Image Correlation*, SAE International Journal of Materials and Manufacturing, vol. 16, no. 3, doi: 10.4271/05-16-03-0019.

[5] "ISO 12004-2:2021 - Metallic materials — Determination of forming-limit curves for sheet and strip — Part 2: Determination of forming-limit curves in the laboratory".

[6] G. Huang, S. Sriram, and B. Yan ,2008, *Digital image correlation technique and its application in forming limit curve determination*, in Proceedings of the IDDRG 2008 International

Conference, Olofstrom, Sweden, pp. 16–18.

[7] W. Volk and P. Hora, 2011, *Evaluation of Experimental Forming Limit Curves and Investigation of Strain Rate Sensitivity for the Start of Local Necking*, AIP Conf Proc, vol. 1383, no. 1, p. 99, doi: 10.1063/1.3623598.

[8] W. Hotz, M. Merklein, A. Kuppert, H. Friebe, and M. Klein, 2013, *Time Dependent FLC Determination Comparison of Different Algorithms to Detect the Onset of Unstable Necking before Fracture*, Key Eng Mater, vol. 549, pp. 397–404, 2013, doi: 10.4028/www.scientific.net/kem.549.397.

[9] M. Merklein, A. Kuppert, and M. Geiger, 2010, *Time dependent determination of forming limit diagrams*, CIRP Annals, vol. 59, no. 1, pp. 295–298, doi: 10.1016/J.CIRP.2010.03.001.

[10] A. J. Martínez-Donaire, F. J. García-Lomas, and C. Vallellano, 2014, *New approaches to detect the onset of localised necking in sheets under through-thickness strain gradients*, Mater Des, vol. 57, pp. 135–145, May 2014, doi: 10.1016/j.matdes.2014.01.012.

[11] J. Min, T. B. Stoughton, J. E. Carsley, and J. Lin, 2017, *An improved curvature method of detecting the onset of localized necking in Marciniak tests and its extension to Nakazima tests*, Int J Mech Sci, vol. 123, pp. 238–252, doi: 10.1016/J.IJMECSCI.2017.02.011.

[12] K. Wang, J. E. Carsley, B. He, J. Li, and L. Zhang, 2014 ,*Measuring forming limit strains with digital image correlation analysis*, J Mater Process Technol, vol. 214, no. 5, pp. 1120–1130, doi: 10.1016/j.jmatprotec.2014.01.001.

[13] J. Min, T. B. Stoughton, J. E. Carsley, and J. Lin, 2017, *Comparison of DIC Methods of Determining Forming Limit Strains*, Procedia Manuf, vol. 7, pp. 668–674, doi: 10.1016/j.promfg.2016.12.099.

[14] L. Huang and M. Shi, 2017, *Determination of the Forming Limit Curve Using Digital Image Correlation - Comparison of Different Approaches to Pinpoint the Onset of Localized Necking*, SAE Technical Papers, vol. -March, doi: 10.4271/2017-01-0301.

[15] Volk, W., & Hora, P. 2011, *New algorithm for a robust user-independent evaluation of beginning instability for the experimental FLC determination*. International journal of material forming, 4, 339-346.

[16] M. A. Sutton, J. H. Yan, V. Tiwari, H. W. Schreier, and J. J. Orteu, 2008, *The effect of out-of-plane motion on 2D and 3D digital image correlation measurements*, Opt Lasers Eng, vol. 46, no. 10, pp. 746–757, doi: 10.1016/j.optlaseng.2008.05.005.